Nuclear Instruments and Methods in Physics Research B 269 (2011) 336–344

Contents lists available at ScienceDirect

Nuclear Instruments and Methods in Physics Research B

journal homepage: www.elsevier.com/locate/nimb

Modification of the mesoscopic structure in neutron irradiated EPDM viewed through positron annihilation spectroscopy and dynamic mechanical analysis

O.A. Lambri [a,b,*,1], F. Plazaola [c], E. Axpe [c], R.R. Mocellini [b], G.I. Zelada-Lambri [b], J.A. García [d], C.L. Matteo [e,1], P.A. Sorichetti [e]

[a] Instituto de Física Rosario – CONICET, Avda. 27 de Febrero 210 bis, 2000 Rosario, Argentina
[b] Facultad de Ciencias Exactas, Ingeniería y Agrimensura, Universidad Nacional de Rosario, Laboratorio de Materiales, Escuela de Ingeniería Eléctrica, Avda. Pellegrini 250, 2000 Rosario, Argentina
[c] Elektrizitatea eta Elektronika Saila, Zientzia eta Teknologia Fakultatea, Euskal Herriko Unibertsitatea, P.K. 644, 48080 Bilbao, Spain
[d] Departamento de Física Aplicada II, Facultad de Ciencias y Tecnología, Universidad del País Vasco, Apdo. 644, 48080 Bilbao, País Vasco, Spain
[e] Departamento de Física, Facultad de Ingeniería, Universidad de Buenos Aires, Avda. Paseo Colón 850, 1063 Buenos Aires, Argentina

ARTICLE INFO

Article history:
Received 9 August 2010
Received in revised form 25 November 2010
Available online 5 December 2010

Keywords:
Mechanical properties
Dynamic mechanical analysis
Positron annihilation spectroscopy
Elasticity theory
EPDM

ABSTRACT

This article focuses on the study of the mesoscopic structure in neutron irradiated EPDM both from experimental and theoretical points of view. In this work we reveal completely the modification of the mesostructure of the EPDM due to neutron irradiation, resolving volume fraction, size and distribution of the crystalline zones as a function of the irradiation dose. Positron annihilation spectroscopy and dynamic mechanical analysis techniques are applied and the results are discussed by means of new theoretical results for describing the interaction process between the crystals and amorphous zones in EPDM.

1. Introduction

The use of polymeric materials for electrical insulators has several advantages: low density, easy handling and good resistance to vandalism. EPDM (ethylene–propylene–diene M-class rubber) among other polymer formulations is a widely used semi-crystalline polymer in organic insulators for watersheds. However, rain, dust deposition, corona effect and ultraviolet radiation, among other environmental agents deteriorate the quality of the polymeric housing, employed as watersheds [1–3]. The knowledge of the physical processes, which control the electrical and mechanical stability of polymers during in-service ageing is critical to predict the long term lifetime of these components. In fact, samples taken from housings of outdoor aged insulators, in-service transmission lines exhibit a decrease in the degree of crystallinity as the ageing time under electric field stress increases [4].

In addition, it has been already reported that neutron irradiation on EPDM leads to the increase in the crystalline degree of this semi-crystalline polymer through a process of chemi-crystallization, which depends on dose and neutron flux level [5,6]. The increase in the volume fraction of crystallites was revealed by means of dynamic mechanical analysis (DMA) response by an increase in the intensity of the maximum of $\tan(\varphi)$, which appears at around 310 K, and that is related to the melting of crystalline zones. In addition, the increase in the size of the crystalline zones was revealed through the shift towards higher temperatures of this maximum [5].

In this work we have performed a new theoretical analysis focused on the change of the elastic energy, which happens due to the different degrees of elastic-misfit between the crystalline and amorphous phases in neutron irradiated EPDM. The new theoretical work is based on a model recently reported for describing the elastic-misfit in two-phase polymers [7]. Besides this, we have realized positron annihilation lifetime spectroscopy (PALS), differential thermal analysis (DTA) and X-ray diffraction (XRD) measurements in neutron irradiated commercial EPDM used as housing of high voltage electrical insulators. The measurements presented here are complemented with a summary of previously reported DMA results (see Refs. [5,6] for details) and discussed on the basis of the theoretical calculations made in the present work. As it will be shown along the paper, DMA and PALS are complementary

* Corresponding author at: Instituto de Física Rosario – CONICET, Facultad de Ciencias Exactas, Ingeniería y Agrimensura, Universidad Nacional de Rosario, Laboratorio de Materiales, Escuela de Ingeniería Eléctrica, Avda. Pellegrini 250, 2000 Rosario, Argentina. Tel.: +54 341 480 26 49/50x125, fax: +54 341 4821772.
E-mail address: olambri@fceia.unr.edu.ar (O.A. Lambri).
[1] Member of the CONICET's Research Staff.

0168-583X/$ - see front matter © 2010 Elsevier B.V. All rights reserved.
doi:10.1016/j.nimb.2010.11.095

techniques very suitable to reveal completely the mesostructure of a two-phase polymer, as the EPDM.

2. Theoretical background

2.1. Positron annihilation lifetime spectroscopy (PALS)

In recent years PALS has shown to be a very good tool to study the free-volume properties of polymers [8]. In the case of polymers positrons also form positronium, Ps (a bound atom which consists of an electron and the positron). Because of the relatively small size of Ps (1.59 Å) compared to other probes, PALS is particularly sensitive to small holes and free volumes in sizes $\leqslant 1$ nm, capable of determining the holes and free volume in a polymer without being perturbed by the solid fraction. In molecular systems, a large fraction of Ps formation is observed in the free-volume regions. The long lifetime of o-Ps (ortho-Ps, the triplet state), that is localised in the free-volume holes, makes it possible to correlate the dimension of the holes with the measured lifetime.

Following the common interpretation of PALS measurements in polymers, the long-lifetime component (τ_3) is associated with ortho-Ps annihilation by pick-off process. From that, the mean size of the holes forming the free volume can be roughly estimated by means of the Eldrup model [9]. In such a model, the ortho-Ps lifetime, τ_3, as a function of the free-volume radius, R, is given by,

$$\tau_3 = 0.5\left[1 - \frac{R}{R_0} + \frac{1}{2\pi}\sin\left(\frac{2\pi R}{R_0}\right)\right]^{-1} \quad (1)$$

where $R_0 = R + \Delta R$ and τ_3 is given in nanoseconds. The radius ΔR is an empirical parameter whose best-value obtained fitting all known data is 1.656 Å [10]. The mean free-volume hole size, V_f, assuming a spherical form for the holes, may be estimated by means of the following equation:

$$V_f = (4\pi/3)R^3 \quad (2)$$

The experimental data of a positron lifetime experiment in polymers are the convolution of three exponentials decays (i.e. three different lifetimes) with the resolution function of the spectrometer. Each lifetime corresponds to the average annihilation rate of a positron in a different state: the shortest and the intermediate lifetimes have contributions from the singlet para-positronium (p-Ps; $\tau_1 \approx 0.12$ ns) and positron annihilation in different molecule species; on the other hand, the longest lifetime ($\tau_3 \geqslant 1$ ns) is due to o-Ps localised in free-volume holes. In this analysis, the τ_3 component is used to determine the mean free-volume hole size. The relative intensity corresponding to this lifetime, I_3, contains information related to the number of the free-volume holes. In this sense, combining the number (I_3) and size (τ_3) of free-volume holes an estimation of the free volume fraction (f) could be extracted [11]:

$$f = AV_fI_3 \quad (3)$$

where A is a proportionality constant, which can be determined by calibrating with other physical parameters [12,13]. However, it is difficult to know the value of A for many polymers. So, Li et al. [14] have defined an apparent fractional free volume (f_{app}) by the following equation:

$$f_{app} = V_fI_3 \quad (4)$$

On the other hand, some authors have shown that I_3 depends also on other variables as activity of the positron source and the chemical composition of the polymer [15–17] as well as elapsed times for temperatures far below T_g [17,18], so, I_3 could not uniquely be ascribed to the free-volume hole number. Taking into account these comments, the absolute value of free volume fraction would not be available from I_3. But taken into account that in this respect the aim of the PALS study is to know the variation of free volume fraction with neutron irradiation dose in the same polymer, EPDM, at room temperature using the same positron source, f_{app} would be an adequate magnitude in order to estimate the free fractional volume variation.

2.2. Elastic misfit in two-phase polymers

We will summarize in this section the essential concepts of the previously reported model for the elastic misfit in two-phase polymers, in order to help to understand the new work. The one-dimensional case only will be presented in this paper; see for more details Ref. [7]. The model takes the idea of partitioning the volume of the sample in small elementary cubes in such a way that each partitioned element is composed by a single phase (amorphous or crystalline in the polymer material we are dealing with). The crystallites are here the inclusions embedded into a continuous and homogeneous matrix, which is represented by the amorphous phase.

Fig. 1 summarizes the main concepts to take into account. It shows a (z, y) plane of the partitioned sample at $x = v$, where the size of the partitioned matrix, over each axis, was chosen equal to lo_p. The model for calculating the degree of the strain misfit starts with the following considerations:

(a) The volume element located at (v, m, j) of the whole partitioned matrix (see for more details Ref. [7]), which is plotted by means of full fine lines in Fig. 1, is cut and removed out of the matrix; leading to a cubic hole of edge lo_p. In other words, a cubic volume is cut from the non-distortioned initial cubic lattice.
(b) An inclusion of size $lo_p + \epsilon lo_p$, with $0 \leqslant \epsilon \leqslant 1$, plotted by means of broken lines will be firstly compressed to fit into the hole of the matrix and subsequently placed in.
(c) The inclusion is mechanically released and then the boundaries of the hole, in the x, y and z axes, displace to a position $lo_p + \beta\epsilon lo_p$, with $0 \leqslant \beta \leqslant 1$, where the equilibrium of stresses is achieved. The wide lines in Fig. 1 represent this state.

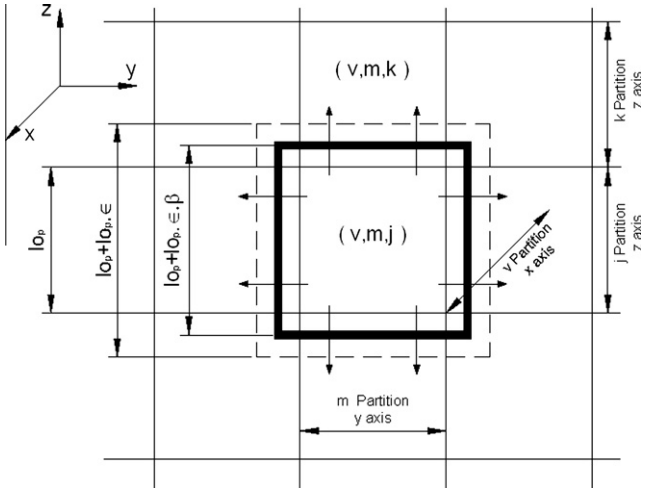

Fig. 1. Accommodation of the misfit strain by the appearance of an inclusion into the material matrix, case: inclusion larger in size than the size of the hole. Fine full line: initial size of the base of the cube of the partitioned material. Broken line: size of the inclusion free of stresses. Wider full line: equilibrium position of the boundary between the inclusion and the matrix, after location of the inclusion into the matrix hole (see details in the text). Arrows in the figure indicate the compression effect of the inclusion on the matrix. Taken from Ref. [7].

It has to be noticed that in this model the inclusion was considered to be larger in size than the hole of the matrix, giving rise to compression stresses into the matrix and into the inclusion, as it was clearly shown in Fig. 1.

The movement of each boundary is considered in each axis as a plane front, which moves until the equilibrium of stresses in each axis is reached.

We will consider now, the movement of the boundary in the z-axis, produced by the inclusion located at (v, m, j) and its effects over the neighbour matrix element (v, m, k), see Fig. 1. The displacement of the boundary of the element (v, m, j) from the initial position (cube in dashed line in Fig. 1) after the inclusion is forced into the hole and released mechanically achieving the mechanical equilibrium, leads to the movement of the front from the solid line to the wider line, Fig. 1.

We consider that the inclusion and the matrix are homogeneous media, and due to the symmetry of the problem the centre of the inclusion will not change its position during the deformation process and the achievement of the stresses equilibrium [7]. Then any point inside the inclusion between the initial state (original size, free of stresses, state represented by the dashed line in Fig. 1) and after forcing the inclusion into matrix and subsequent achievement of the mechanical equilibrium, moves from $(z + z\epsilon)$ to $(z + z\epsilon\beta^z)$, where β^z means the misfit coefficient along the z-axis. This leads to a displacement in the z-axis, $u_i(z)$, that is

$$u_i(z) = (z + z \cdot \epsilon) - (z + z \cdot \epsilon \cdot \beta^z) \tag{5}$$

$$u_i(z) = z\epsilon(1 - \beta^z) \tag{6}$$

Consequently the mean strain inside the inclusion (averaged by the mean field approximation) in the z-axis, ϵ_i^z, results,

$$\varepsilon_i^z = \frac{\partial u_i}{\partial z} = \epsilon(1 - \beta^z) \tag{7}$$

Hereafter, the magnitudes corresponding to the inclusion or to the matrix, will be noted with a subscript i or m; respectively. In addition, in order to keep the same style of the mathematical notation used in the work of Ref [7], either the direction for the strain misfit coefficient, β, and for the number of inclusions or matrix elements (N) will be denoted through a supra-subscript.

On the other hand, we obtain now the resulting mean strain inside the matrix element. Let us consider that there exists an inclusion concentration lying in the z-axis N_i^z/N_m^z (where N_i^z and N_m^z are the number of inclusions and the number of matrix elements, respectively, which satisfy the condition $N_i^z + N_m^z = N_z$), the N_i^z inclusions move the boundaries of the N_m^z partitions, in such a way that to the partition (v, m, k) corresponds the following displacement $z + z\epsilon\beta^z N_i^z/N_m^z$. Then, the displacement in the z-axis for the matrix elements can be written as

$$u_m(z) = z \cdot \epsilon \cdot \beta^z \left(\frac{N_i^z}{N_m^z}\right) \tag{8}$$

Therefore, the strain inside the matrix element in the z-axis, ε_m^z, results,

$$\varepsilon_m^z = \frac{\partial u_m}{\partial z} = \epsilon \cdot \beta^z \left(\frac{N_i^z}{N_m^z}\right) \tag{9}$$

By working Eq. (9) we obtain,

$$\varepsilon_m^z = \epsilon \cdot \beta^z \left(\frac{N_i^z/N^z}{N_m^z/N^z}\right) = \epsilon \cdot \beta^z \frac{fr_i^z}{fr_m^z} \tag{10}$$

where fr_i^z and fr_m^z are the volume fraction for the inclusions and matrix element in the z-axis, respectively.

From the mechanical equilibrium conditions at the boundary between the adjacent elements (v, m, j) and (v, m, k), according to the Reuss approximation [7,19] and by applying the Hooke's law; the misfit coefficient in the z-axis, β^z, can be obtained as a function of the Young moduli, E, and volume fraction of both inclusions and matrix,

$$\beta^z = \frac{1}{1 + \left(\frac{E_m}{E_i}\right) \cdot \left(\frac{fr_i^z}{fr_m^z}\right)} \tag{11}$$

Moreover, considering that the distribution of inclusions is random in the bulk matrix, it can be demonstrated easily that [7]

$$\beta^z = \beta^x = \beta^y = \beta \tag{12}$$

Indeed, β is the misfit coefficient, which relates the inclusion strain caused by the matrix (or vice versa). The larger the strain over the inclusion, the lower the value of β.

3. Experimental

3.1. Samples

Samples were taken from commercial ethylene–propylene–diene M-class rubber (EPDM) used as housing of non-ceramic electrical insulators (Avator of Sitece Electrical Industries, Buenos Aires, Argentina), which are employed in outdoor transmission lines of 66 kV [1–4]. The nominal molar composition of the rubber was 55% ethylene–42% propylene and 3% diene-monomer. The EPDM used in the present work was reinforced with ceramic particles of Bayerite (alumina-trihydrate, ATH) in a proportion of 44 wt%, as it is usual for electrical applications in order to improve the flashover resistance. See for more details Refs. [1–4].

3.2. Neutron irradiation

Neutron irradiations were performed under different conditions in two different nuclear reactors, the RA-6 and the RA-4 of the National Atomic Energy Commission of Argentina, where the main differences were the flux level and power of operation. In both reactors the samples were irradiated at room temperature in air at atmospheric pressure.

Samples irradiated at the RA-6 nuclear reactor will be identified as samples under high flux irradiation. All samples were irradiated with bismuth and cadmium filters. The doses and fluxes related to neutron irradiation are written in Table 1.

In the RA-4 reactor, the samples were placed inside of a cylinder of poly-methyl-methacrylate (PMMA) of 250 mm length and 25 mm diameter with wall and bases of thickness of 2 mm and 20 mm, respectively. Samples irradiated at the RA-4 nuclear reactor will be identified as samples under low flux irradiation, for more details see Table 1 and Refs. [5,6,20].

Table 1
Status of the studied samples, detailing the doses and neutron fluxes used during the neutron irradiation processes.

Sample denomination	Dose (Gy)	Thermal neutron flux (n/cm^2 s)	Fast neutron flux (n/cm^2 s)
A	0	0	0
High flux irradiation			
H	415	8.5×10^7	2.75×10^8
I	830	"	"
J	4150	1.7×10^8	5.5×10^8
K	8300	"	"
Low flux irradiation			
C	12.7	5.7×10^7	5.0×10^7
E	38.2	"	"
F	51.0	"	"

Table 2
Positron lifetime results in neutron irradiated samples under high flux conditions. The fitting of the spectra has been performed using the LT program and a continuous distribution of the long component, whose average lifetime and intensity are $\langle\tau_3\rangle$ (ps) and I_3, respectively. σ is the standard deviation of the long component. τ_1 and τ_2 are the shorter lifetime components and I_2 the intensity of the middle one.

Dose (Gy)	τ_1 (ps)	τ_2 (ps)	I_2 (%)	$\langle\tau_3\rangle$ (ps)	σ (ns)	I_3 (%)	χ^2
0	225 ± 8	471 ± 22	36.4 ± 2.4	2544 ± 75	0.71 ± 0.10	17.8 ± 0.9	1.06
415	260 ± 4	570 ± 66	10.2 ± 1.7	2470 ± 78	0.79 ± 0.12	13.8 ± 0.6	1.00
830	244 ± 1	479 ± 8	22.7 ± 0.3	2544 ± 46	0.73 ± 0.05	16.1 ± 0.2	1.01
8300	230 ± 2	479 ± 7	33.7 ± 0.8	2554 ± 16	0.67 ± 0.03	19.4 ± 0.3	1.03

Table 3
Positron lifetime results in neutron irradiated samples under low flux conditions. The fitting of the spectra has been performed using the LT program and a continuous distribution of the long component, whose average lifetime and intensity are $\langle\tau_3\rangle$ (ps) and I_3, respectively. σ is the standard deviation of the long component. τ_1 and τ_2 are the shorter lifetime components and I_2 the intensity of the middle one.

Dose (Gy)	τ_1 (ps)	τ_2 (ps)	I_2 (%)	$\langle\tau_3\rangle$ (ps)	σ (ns)	I_3 (%)	χ^2
0	225 ± 8	471 ± 22	36.4 ± 2.4	2544 ± 75	0.71 ± 0.10	17.8 ± 0.9	1.06
12.7	236 ± 4	430 ± 22	25.4 ± 2.5	2458 ± 39	0.82 ± 0.05	14.8 ± 0.7	1.01
38.2	217 ± 9	447 ± 18	39.0 ± 2.4	2506 ± 56	0.88 ± 0.07	18.6 ± 0.9	1.00
51	255 ± 5	519 ± 44	16.6 ± 2.3	2551 ± 71	0.73 ± 0.10	15.5 ± 0.7	1.08

3.3. Measurements

Positron lifetime measurements were performed by a conventional fast–fast timing coincidence system with a resolution (full width at half maximum) of 240 ps. As positron source a ^{22}NaCl source of about 15 μCi evaporated onto a thin Kapton foil was used. As we have only one irradiated sample corresponding to the particular neutron dose under study, the positron source was sandwiched between the sample under study and a well-annealed Al sample. To obtain the source correction two well-annealed Al samples were used. The source correction used to fit the polymer spectra was composed by two contributions: one corresponding to the Al contribution to the spectra: 165 ps/43.5% and the other one corresponding to the Kapton source: 382 ps/13%. The number of counts on all measured spectra was always around 4 million counts. All lifetime spectra were analyzed in three components after subtracting the source contribution. We have used the LT_92_3 program [21] to fit the spectra with a continuous distribution of positron lifetimes for the long lifetime τ_3. The lifetime data corresponding to the fitting procedure are presented in Tables 2 and 3. In the present work we are interested in the evolution of the average of the free volume; so, we have particularly analyzed the parameters of the long component, lifetime and intensity, which are related to an average of free volume distribution present in the sample.

Differential Thermal Analysis, DTA, measurements were performed in a conventional calorimetric equipment employing stainless steels crucibles under argon at atmospheric pressure. The employed heating rates were 2, 5, 7, 10 and 15°/min, starting from liquid nitrogen temperatures.

X-rays diffraction, XRD, measurements were carried out employing a X-Pert Phillips 5000 powder diffractometer working in reflection mode at room temperature. The Cu ($K\alpha_1$) wavelength (λ = 1.540562 A^{-1}), with monochromator, was used as incident radiation. The measurement conditions were: acceleration voltage: 40 kV, filament current: 20 mA, step in 2θ: 0.02° and the counting times were: 5, 20 and 50 s (in each 2θ step).

Measurements of dynamic mechanical analysis, DMA, loss tangent (damping), tan(φ), and elastic shear modulus, G', were carried out as a function of temperature at frequencies between 1 and 70 Hz. The temperature range of the measurements was between 180 K and 370 K and the heating rate was 1 K/min. Measurements were performed under Argon atmosphere at atmospheric pressure. The samples for DMA studies were parallelepiped bars of 5 mm width, 4 mm thick and 30 mm length. The maximum shear strain on the sample was 2×10^{-4}. tan(φ) values were independent of the amplitude of the oscillating strain, i.e. doubling the applied stress led to the doubling of the strain response [22]. The estimated uncertainties for tan(φ) and G' were less than 3% and 10%, respectively. For all the measured samples the oscillating frequency was close to 4 Hz. See Refs. [5,6] for more experimental details.

4. Results and discussion

4.1. Elastic misfit for an inclusion smaller than the hole

In this Section we develop the concepts and equations related to the misfit of strain in a two-phase polymer, presented in Section 2.2, when the inclusion has a size smaller than the hole in the matrix.

Fig. 2 summarizes the main concepts to take into account for this new case under study. As in Section 2.2, it shows a (z, y) plane of the partitioned sample at $x = v$, where the size of the partitioned matrix, over each axis, was chosen equal to lo_p. The model now starts with the following considerations:

(a) The volume element located at (v, m, j) of the whole partitioned matrix, which is plotted by means of full fine lines in Fig. 2, is cut and removed out of the matrix; leading to a cubic hole of edge lo_p.
(b) An inclusion of size $lo_p - \epsilon lo_p$, with $0 \leqslant \epsilon \leqslant 1$, plotted by means of broken lines will be placed into the hole of the matrix, surrounded by glue, and then the matrix is compressed up to be pasted.
(c) The matrix is mechanically released and then the boundaries of the hole, in the x, y and z axes, displace to a position $lo_p - \beta\epsilon lo_p$, with $0 \leqslant \beta \leqslant 1$, where the equilibrium of stresses is achieved. The wider lines in Fig. 2 represent this state.

We will use the same considerations from the elastic point of view that were used in Section 2.2. Similarly we will consider, the movement of the boundary in the z-axis, produced by the inclusion located at (v, m, j) and its effects over the neighbour matrix element (v, m, k), Fig. 2. The displacement of the boundary of the element (v, m, j) from the initial position (cube in dashed line in Fig. 2) after the inclusion is pasted to the matrix and released

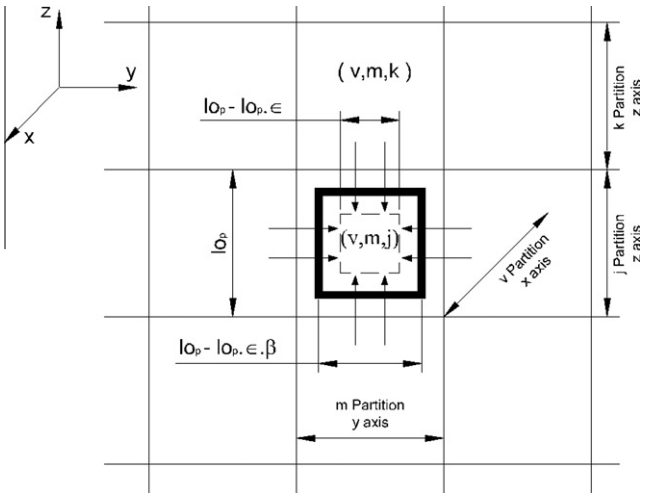

Fig. 2. Accommodation of the misfit strain by the appearance of an inclusion into the material matrix, case: inclusion smaller in size than the size of the hole. Fine full line: initial size of the base of the cube of the partitioned material. Broken line: size of the inclusion free of stresses. Wider full line: equilibrium position of the boundary between the inclusion and the matrix, after location of the inclusion into the matrix hole (see details in the text). Arrows in the figure indicate the stretching effect of the inclusion on the matrix.

mechanically achieving the mechanical equilibrium, leads to the movement of the front from the solid line to the wider line, Fig. 2.

As it can be easily deduced, the displacement in the z-axis, $u_i(z)$, is for the present case

$$u_i(z) = (z - z\cdot\epsilon\beta^z) - (z - z\cdot\epsilon) \tag{13}$$

$$u_i(z) = z\epsilon(1-\beta^z) \tag{14}$$

As it can be deduced comparing Eq. (14) and Eq. (6), the absolute values for the displacement are the same. Consequently the mean strain inside the inclusion (averaged by the mean field approximation) in the z-axis, ε_i^z, results equal to Eq. (7), that is

$$\varepsilon_i^z = \frac{\partial u_i}{\partial z} = \epsilon(1-\beta^z) \tag{15}$$

Therefore, the β coefficient takes the same form than in Eq. (11), as it can be easily shown.

4.2. Elastic energy produced by the strain misfit

It is well known that the relation between the stress and strain tensors is given by means of the Cauchy equation in the usual form, as [23]

$$\sigma_{ij} = C_{ijkl}\varepsilon_{kl} \tag{16}$$

where C_{ijkl} is the elastic modulus. In addition, the elastic strain density is given by the expression

$$w = \frac{1}{2}\int \sigma_{ij}d\varepsilon_{ij} = \frac{1}{2}\int C_{ijkl}\varepsilon_{kl}d\varepsilon_{ij} \tag{17}$$

In the next paragraphs we will refer to the deformation ε and to a β coefficient for the case of compression of the inclusion and the matrix, only for the simplicity in the mathematical signs. However, the analysis made below is indistinctly for the compression or tensile state of the inclusions and matrix, because we are dealing with the misfit phenomenon independently of the type of forces that give rise to the relaxation.

By considering a homogeneous media in the one-dimensional case and using the notation for the components lying over an axis as in previous sections, we can write for the z-axis,

$$w^z = \frac{1}{2}E(\varepsilon^z)^2 \tag{18}$$

The initial strain imposed to the element of inclusion (v, m, j) for fixing it into the hole of the matrix is given by considering $\varepsilon_i^z = \epsilon$ (see Fig. 1), then the elastic strain density of the inclusion for the initial state of deformation, in the z-axis, results

$$w_i^z = \frac{1}{2}E_i\cdot\epsilon^2 \tag{19}$$

The whole elastic energy available to be transferred to one matrix element over the z-axis is

$$W_T^z = \frac{1}{2}E_i\cdot\epsilon^2\cdot V_p\cdot\left(\frac{N_i^z}{N_m^z}\right) \tag{20}$$

where V_p is the volume of the (v, m, j) partition and $N_i^z + N_m^z = N^z$, as meant in the previous section. Multiplying and dividing by N^z, we have

$$W_T^z = \frac{1}{2}E_i\cdot\epsilon^2\cdot V_p\cdot\left(\frac{N_i^z/N^z}{N_m^z/N^z}\right) = \frac{1}{2}E_c\cdot\epsilon^2\cdot V_p\cdot\left(\frac{fr_i^z}{fr_m^z}\right) \tag{21}$$

and by working the above equation, it is easy to show that we can write,

$$W_T^z = \frac{1}{2}E_i\cdot\epsilon^2\cdot V_p\cdot\left(\frac{fr_i^z}{1-fr_i^z}\right) \tag{22}$$

On the other hand, the density of elastic energy transferred to the matrix, in the z-axis, after the releasing the inclusion into it is

$$w_m^z = \frac{1}{2}E_m\cdot(\varepsilon_m^z)^2 \tag{23}$$

with ε_m^z given by the value in Eq. (10) in Section 2.2. So, the energy density for the matrix partition can be written as

$$w_m^z = \frac{1}{2}E_m\epsilon^2\cdot\beta^2\left(\frac{fr_i^z}{1-fr_i^z}\right)^2 \tag{24}$$

The energy in the partition corresponding to the matrix element results

$$W_m^z = \frac{1}{2}E_m\epsilon^2\cdot\beta^2\left(\frac{fr_c}{1-fr_c}\right)^2\cdot V_p \tag{25}$$

As the volume of the partitions is the same, the ratio between the density of elastic energy and the elastic energy itself is the same, that is $W_m^z/W_T^z = w_m^z/w_T^z$, therefore the ratio between the elastic energy transferred to the matrix and the whole available one is

$$\frac{w_m^z}{w_T^z} = \frac{E_m}{E_i}\beta^2\left(\frac{fr_i^z}{1-fr_i^z}\right) \tag{26}$$

It is convenient to mention again that the transfer of elastic energy is due to the movement of the borders of the inclusion into the matrix from its initial compressed state up to the achievement of the mechanical equilibrium condition.

In another light calling

$$SF = \frac{E_m}{E_i}\left(\frac{fr_i^z}{1-fr_i^z}\right) \tag{27}$$

Eq. (26) can be written as

$$\frac{w_m^z}{w_T^z} = SF\beta^2 \tag{28}$$

By replacing the expression for β given by Eq. (11) in Section 2.2, we can write

$$\beta^2 = \frac{1}{(1+SF)^2} \tag{29}$$

and then

$$\frac{w_m^z}{w_T^z} = \frac{SF}{(1+SF)^2} \tag{30}$$

Taking the derivative of the expression (30) with respect to the volume fraction of inclusions we have,

$$\frac{\partial}{\partial fr_i}\left(\frac{w_m^z}{w_T^z}\right) = \frac{\partial}{\partial fr_i}\left(\frac{SF}{(1+SF)^2}\right) \tag{31}$$

and paying attention to the fact that

$$\frac{\partial SF}{\partial fr_i^z} = \frac{E_m}{E_i}\left(\frac{1\cdot(1-fr_i^z)-fr_i^z(-1)}{(1-fr_i^z)^2}\right) = \frac{E_m}{E_i}\cdot\frac{1}{(1-fr_c^z)^2} \tag{32}$$

and to the fact that

$$SF|_{fr_i^z=0} = \frac{E_m}{E_i}\left(\frac{fr_i^z}{1-fr_i^z}\right)\Big|_{fr_i^z=0} = 0 \tag{33}$$

with

$$\left.\frac{\partial SF}{\partial fr_i^z}\right|_{fr_i^z=0} = \frac{E_m}{E_i}\cdot\left.\frac{1}{(1-fr_i^z)^2}\right|_{fr_i^z=0} = \frac{E_m}{E_i} \tag{34}$$

we obtain that

$$\frac{\partial}{\partial fr_i}\left(\frac{w_m^z}{w_T^z}\right)\Big|_{fr_i^z=0} = \frac{E_m}{E_i} \tag{35}$$

Then, the derivative of the ratio between w_m^z and w_T^z evaluated at zero volume fraction of inclusions, allows us to know the ratio between the elastic modulus of the matrix and inclusions.

Assuming that the elastic modulus of the crystalline zones does not change appreciably with the size of the crystal, the behavior of the elastic modulus of the matrix can be easily obtained from Eq. (35). We have obtained for all the samples detailed in Table 1, results from Eq. (35), which are in good agreement with the previous reported work of Ref. [5]. Indeed, it represents a mathematical closure condition.

4.3. Experimental results

Fig. 3 shows the behavior of crystal size (left axis) and free-volume hole (V_f) of the EPDM rubber (right axis) as a function of irradiation dose, for the high flux irradiated samples. The free volume of the rubber was determined from PALS measurements and the crystal size was determined from DMA tests [5]. The free-volume hole decreases after irradiating the sample with a dose of 415 Gy. Even though the error bars of the measurements do not allow deciding definitely the free volume behavior, they suggest a free volume decrease in the sample. The decrease in the values of the crystal size for a dose of 415 Gy was earlier related to the destruction of the initial crystalline degree of the as-received rubber, by the neutron irradiation [5]. In addition, the re-increase in the crystal size (increase of the temperature of tan(φ) peak, T_p) at higher doses (830 Gy and higher) in Fig. 3, was related to the re-building of a crystalline state through a chemi-crystallization process [5,6,24–28]. As it is well known, EPDM is a semi-crystalline polymer where the chains are composed by a random arrangement of ethylene, propylene and diene monomers, which are very weakly polar. The propylene and diene monomers are slightly more polar than ethylene.

Besides, chains having predominantly long sequences of ethylene groups compose the crystalline zones in EPDM [1,2,4,29,30].

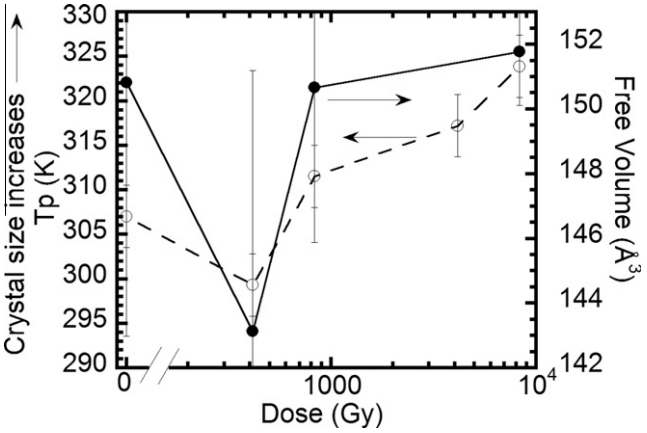

Fig. 3. Left axis: temperature of the tan(φ) maximum (T_p), empty circles. Right axis: free volume, full circles. High flux irradiated samples.

Neutron irradiation produces chain scissions, the scission products having less restricted mobility. Disentanglement of such fragments allows them to crystallize into imperfect, low-melting point crystals, increasing the overall crystalline content. The crystal size increase caused by the process of chemi-crystallization during irradiation was explained on the basis of crystal growing, related to small inclusions/matrix interface energy decrease [5].

Due to the experimental error bars in the values of V_f (see Fig. 3) it is not possible to reveal clearly its trend and therefore, its relation with the change in size of the crystals in the matrix during the development of the re-building of the crystalline state by chemi-crystallization, at doses higher than 415 Gy. However, we could establish that the size of the holes is the smallest one at 415 Gy where the destruction of the crystalline state has taken place.

Fig. 4 shows both the behavior of the crystalline volume fraction and the apparent fractional free volume ($V_f \times I_3$) in the rubber as a function of the irradiation dose, for the high flux irradiated samples. The apparent fractional free volume in the rubber was determined from PALS and the crystalline volume fraction was determined from the intensity of tan(φ) peak [5].

It can be concluded from the measurements in Figs. 3 and 4 that: (a) as the crystal size increases, the free volume seems to increase too (Fig. 3) and (b) the increase in the crystalline volume fraction is accompanied by an increase in the apparent fractional free volume of the sample and vice versa (Fig. 4).

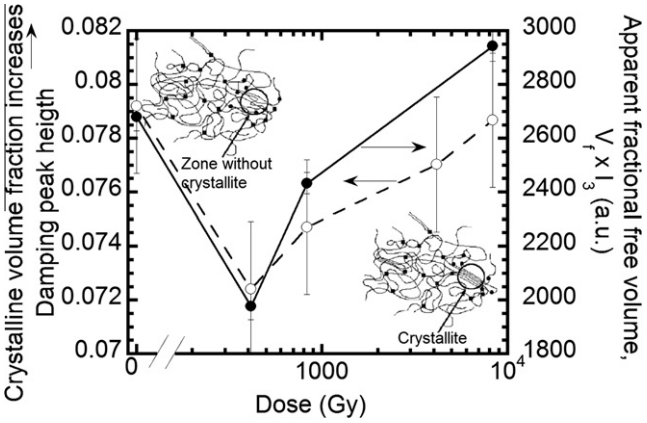

Fig. 4. Left axis: tan(φ) maximum, empty circles. Right axis: apparent fractional free volume, full circles. High flux irradiated samples. Drawings inserted in the figure show the destruction of the crystallinity at 415 Gy, and its restoration at higher doses, see explanation in the text.

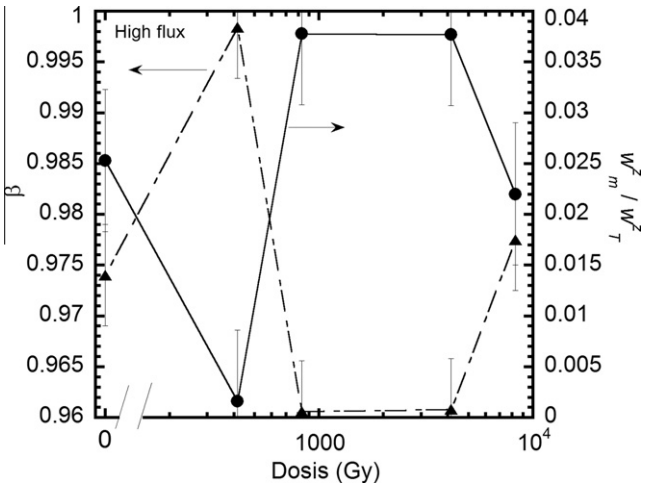

Fig. 5. Left axis: misfit coefficient β calculated using Eq. (11). Right axis: ratio w_m^z/w_T^z calculated from Eq. (26). High flux irradiated samples.

Now we will consider the behavior of both the coefficient β, calculated from Eq. (11), and the ratio w_m^z/w_T^z, calculated from Eq. (26), as a function of the irradiation dose; for the high flux irradiated samples, Fig. 5. The initial state of the rubber exhibits a coefficient β with a value close to 0.975 and a w_m^z/w_T^z value close to 0.025. Subsequently for a dose of 415 Gy, where either crystal size and crystals volume fraction decrease (see Figs. 3 and 4), β increases to a value close to 1 meanwhile w_m^z/w_T^z decreases to a value close to 0.001. The β increase is indicating that the stresses into the matrix promoted by the accommodation of the strain misfit produced by the crystals have decreased substantially. It is in agreement with the decrease in w_m^z/w_T^z due to the very small energy transferred to the amorphous phase, w_m^z from the inclusions misfit, w_T^z. In addition, increasing the dose, both crystal size and crystalline volume fraction start to re-increase due to chemi-crystallization process promoted by the neutron irradiation and then β decreases and w_m^z/w_T^z increases.

Comparing the behavior of the free-volume hole (V_f) and β we observe that when V_f decreases, β increases and vice versa. Therefore, the physical mechanism that controls this behavior, at mesoscopic level, in the EPDM matrix can be related to inclusions with size smaller than the hole on the matrix. In fact, as it was shown in Section 4.1, this situation leads to a tensile state, both in the inclusion (crystal) and in the matrix. Indeed, at the destruction of the crystalline state at 415 Gy, the free volume achieves the smallest value, since the tensile state both in the matrix and crystals have disappeared and then the relaxation of the internal tensile stresses into the matrix leads to β close to 1. By increasing the irradiation dose over 415 Gy, the crystals are re-built, with a size smaller than the hole in the host matrix, and then the field of internal stresses is restored leading to both: (a) the increase in V_f, since the matrix is now stretched, and (b) the decrease in β, since the appearance of internal stresses. Indeed, the appearance of the crystals growth give rise to an increase in the internal stresses and consequently it leads to an increase in the elastic energy of the matrix, revealed by the decrease of β and the increase of w_m^z/w_T^z, respectively.

Therefore, from coupling the results of the behavior of the β coefficient and w_m^z/w_T^z, obtained from the theoretical results and the changes in the free volume, measured by PALS, we can suggest that the changes of the empty spaces within the rubber are promoted by the appearance of internal tensile stresses promoted by the development of the chemi-crystallization.

The last increase in β together with the last decrease of w_m^z/w_T^z for a dose of 8300 Gy, is related to a large deterioration of the rubber matrix by chain scission owing to the neutron irradiation, which is accompanied by a strong reduction of the elastic modulus of the matrix [5].

As it can be seen from Fig. 5, the behavior of the β coefficient is the reciprocal of the ratio w_m^z/w_T^z. In addition, a goal should be emphasized from the new theoretical calculations, that is, the behavior of the ratio w_m^z/w_T^z for studying the evolution of the internal stresses, and consequently the empty space, in a polymer matrix is more sensitive than β coefficient. In fact, the largest variation in β from Fig. 5 is about 4%, meanwhile for w_m^z/w_T^z it is almost of one order of magnitude.

In addition, it is convenient to remember that in the results of Fig. 5, β and w_m^z/w_T^z reflect the accommodation effects owing to the collective strain misfit, produced by the whole group of inclusions within the rubber, independently of the inclusion size (larger or smaller) respect to the hole in the matrix.

The increase of the apparent fractional free volume within the rubber is related to the increase of the volume fraction of crystals promoted by chemi-crystallization. In Fig. 4, two very simplified 2D views of the semi-crystalline rubber [4,30], accordingly to the stages controlled by irradiation, are inserted. In fact, after irradiating to a dose of 415 Gy the crystalline degree is reduced, and the sample is more amorphous than at the non-irradiated state. However, after further irradiation to higher dose, the crystalline state develops by chemi-crystallization and the polymer becomes again less amorphous. It is interesting to notice that the intensity of the second lifetime component (I_2), shown in Table 2, is in very good agreement with the previous behavior, reinforcing the scheme drawn in Fig. 4. I_2 decreases abruptly after irradiating the EPDM sample with a dose of 415 Gy (the intensity decreases from about 35% to 10%), when the sample becomes more amorphous. For larger irradiation doses (the sample becomes less amorphous) the intensity recovers monotonously towards the value in the non-irradiated EPDM. As chemi-crystallization is produced by piling up of nearby located cut polymer chains of the amorphous matrix, the length of the polymer chains per unit area, within the newly formed crystalline zone, is shorter than when the same zone is amorphous, leading to a less dense matrix. Therefore, the apparent fractional free volume (empty space) increases with the increase in the volume fraction of the crystallites.

Fig. 6 shows the behavior of the crystalline volume fraction determined from the DMA test (see left axis) for the low flux irradiated samples. As it can be seen from the figure, the achieved volume crystal fraction first decreases after a dose of 12.7 Gy and at 38.2 Gy the largest volume fraction is achieved. The apparent fractional free volume ($V_f \times I_3$) determined from PALS is showed in the right axis. It can be seen that the increase in the volume fraction is accompanied of an increase in the apparent fractional free volume and vice versa, similarly as for the case of high dose neutron irradiation.

Curves relating the free volume and the size of the crystals for the case of low flux neutron irradiation are not presented due to the negligible change in the size of crystals obtained from DMA test during the low flux irradiation.

For low dose irradiation the measured crystalline volume fraction is the highest achieved during the irradiations, either at low and high fluxes, and it is also higher than the initial crystalline volume fraction [5]. In fact, it is different to the ones obtained with the high flux irradiation condition where the volume fraction of crystals firstly decreases markedly at 415 Gy and it results close to the initial crystallinity degree for the highest achieved dose of 8300 Gy, see left axis in Fig. 4. In addition, other difference appears between the experiments performed at low and high flux irradiation condition, which is related to the size of the crystals. In the low flux irradiation condition the size of the crystals did not change appreciably as the dose increases during the irradiation

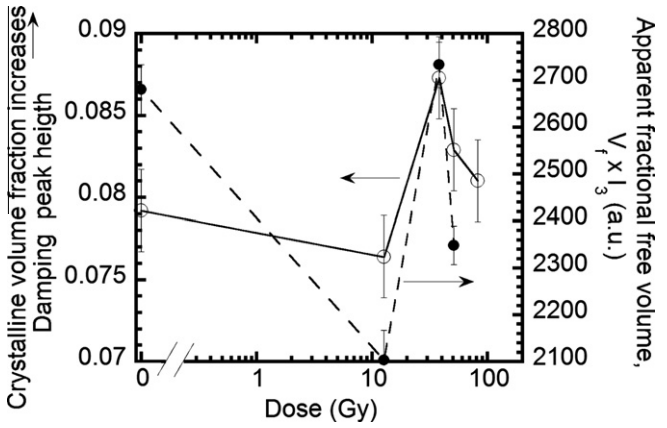

Fig. 6. Left axis: tan(φ) maximum, empty circles. Right axis: apparent fractional free volume, full circles. Low flux irradiated samples.

process. In contrast under the high flux irradiation condition, the size of crystallites increases markedly for doses higher than 415 Gy [5], see left axis in Fig. 3.

Therefore, by coupling low and high flux neutron irradiation conditions we can study the promotion of internal stresses into the rubber matrix, due to two different physical mechanisms. Indeed, at low flux irradiation condition the increase of the mechanical stresses in the rubber is controlled mainly by the increase in the quantity of crystals (crystallite size does not appreciably change), i.e. volume fraction. In contrast, in high flux irradiated samples the increase in the mechanical stresses is controlled mainly by both, the increase in the size of the crystals and in the quantity of crystals.

In the other hand, the behavior of the coefficient β and the ratio w_m^z/w_T^z calculated for the low flux irradiated samples have been plotted in Fig. 7. At 12.7 Gy the deterioration of the initial crystallinity of the rubber in the as-received state occurs, then β tends to 1 and w_m^z/w_T^z tends to 0.001. The largest degree of crystallinity developed by chemi-crystallization, at 38.2 Gy, leads to a decrease in β and to an increase in w_m^z/w_T^z, indicating that internal stresses are produced into the rubber due to the development of the chemi-crystallization and consequently the elastic energy transferred to the amorphous matrix has increased.

The behavior showed in Fig. 7 for the low flux irradiated samples is in agreement with the results showed previously for the case of high flux irradiated samples, even if the promotion of

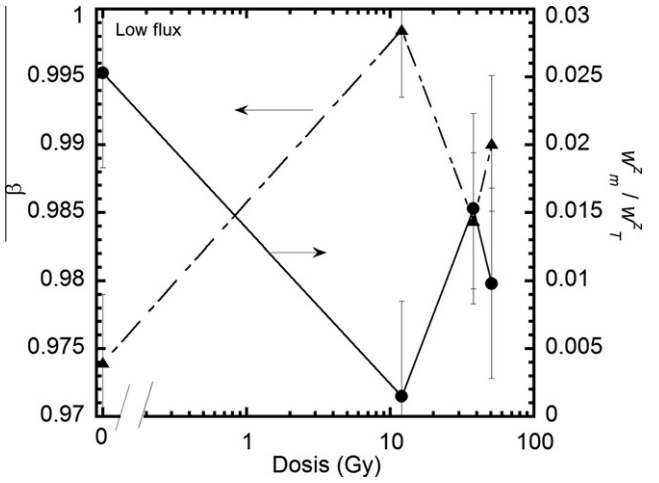

Fig. 7. Left axis: misfit coefficient β calculated using Eq. (11). Right axis: ratio w_m^z/w_T^z calculated from Eq. (26). Low flux irradiated samples.

internal stresses and then the energy transfer to the matrix is controlled by different crystal arrangements in the high and low irradiated samples. Indeed, the results highlight the useful of the new theoretical calculations either, when the mechanical stresses are promoted by the increase in size of the crystallites (inclusions) or when the mechanical stresses are promoted by the increase in the volume fraction of crystallites. As it was already mentioned for the case of high flux irradiated samples, it is convenient to point out here again that the coefficient β and the ratio w_m^z/w_T^z measure the average inclusion strain and the corresponding transferred energy in the whole matrix and vice versa, independently if the inclusion is larger or smaller than the hole in the matrix, see Sections 2.2 and 4.1.

It is interesting to note, that coefficient β and the ratio in w_m^z/w_T^z provide other very valuable information for the case of crystals developed within polymers. In the case of low flux irradiation, the developed crystals by chemi-crystallization (new crystals), with no apparent change on their size, generate a smaller elastic distortion leading to β closer to 1 in the rubber than the previously existing crystals in the as-received state of the rubber, Fig. 7. In addition, the ratio in w_m^z/w_T^z in the low flux irradiated samples is smaller than in the unirradiated state. However, high flux irradiation promotes the growing of larger crystals. They produce internal stresses are larger than the ones caused by the initial crystals presented in the rubber in the as-received state (see Figs. 3 and 5), therefore β is smaller and the ratio w_m^z/w_T^z is larger.

We attempted also to observe the change in the crystallinity promoted by neutron irradiation in EPDM by means of DTA and XRD studies.

DTA thermograms for all the samples detailed in Table 1, exhibited a wide endothermic reaction at around 310–350 K, related to the melting of the crystalline zones; which shape was similar to the ones previously reported [5]. Nevertheless, from the DTA tests, performed at different heating rates (see Section 3.3), we could not detect clear changes between the thermograms recorded for all the kind of samples. The lack of resolution in the thermograms can be related to the small mass involved by the crystals in contrast to the whole mass of the sample.

X-rays diffraction patterns measured for all the samples detailed in Table 1 showed a wide reflection peak at around $2\theta = 18°$, which could be related to the crystalline zones, and also reflections corresponding to the triclinic lattice of the Bayerite (alumina-tri-hydrate, ATH), which appeared overlapped. Nevertheless, clear changes in the integrated intensity of the reflection peak related to the crystals could not be observed, even if the samples were measured using the longest counting time. This lack of discrimination for the XRD measurements is in agreement with the level of resolution of the XRD technique, which depends of the volume fraction and morphology involved. In fact, X-ray diffraction studies have a limit of resolution of about 1–3% of volume fraction involved. Then, we can conclude that the range of diffraction angles employed in XRD studies with Cu (Kα) radiation in that work is not appropriate for detecting these crystals. Indeed, it could be necessary to work at small angles in diffraction studies using X-rays or neutrons [31,32].

The limitations in the resolution of XRD and DTA techniques for studying the change in the crystalline degree promoted by chemi-crystallization process in EPDM, which we found in this work, are in agreement with previously reported works in the literature [27]. However, we have reported recently that dielectric relaxation (DR) measurements can reveal the change in the crystallinity in neutron irradiated EPDM, but DR cannot distinguish if the change in the crystallinity is controlled by a change in the volume fraction or by an increase in the size of the crystals [7]. In addition, the feasibility of employing near infrared spectroscopy, studies to distinguishing between irradiated and unirradiated samples has been already reported in the literature [33,34].

5. Conclusions

The coupling of dynamic mechanical analysis and positron annihilation lifetime spectroscopy experimental techniques, can reveal the mesostructure of the neutron irradiated commercial EPDM, used as housing of electrical insulators, resolving volume fraction, size and distribution of the crystals embedded into the matrix. This result should be emphasized due to the limitations, which appear in other characterization techniques for resolving the changes both in the volume fraction and size of the crystalline zones in EPDM.

The theoretical predictions of the strain misfit coefficient, β, and the energy transfer ratio, w_m^z/w_T^z, allow quantifying the internal stresses state within the EPDM and also give a quantitative connection between the dynamic mechanical analysis and positron annihilation lifetime spectroscopy techniques. In addition, the new theoretical calculations made for the energy transfer ratio, result more sensitive for studying the internal stresses state in EPDM than the misfit coefficient.

Acknowledgements

This work was partially supported by the Collaboration Agreement between the Universidad del País Vasco and the Universidad Nacional de Rosario Res. 1792/2003, UPV224.310-14553/02, Res. 3469/2007 and Res. 124/2010, the CONICET-PIP No. 2098 and 5665, and the PID-UNR (ING 227) 2008–2009 and (ING 288) 2010–2013. We are also indebt to Eusko Jaurlaritza for the support under Grant No. IT-443-10.

References

[1] W.W. Pendleton, in: M.B. Bever (Ed.), Encyclopedia of Materials Science and Engineering, Vol. 2 Co-E, Pergamon Press, Oxford, 1986.
[2] J. Ulanski, M. Kryszewski, Polymers, electrical and electronic properties, in: G. Trigg (Ed.), Encyclopedia of Applied Physics, Vol. 14, VCH Publishers Inc., New York, 1996, p. 497.
[3] R. Hackam, Outdoor HV composite polymeric insulators, IEEE Trans. Dielectr. Electr. Insul. 6 (1999) 557.
[4] P.A. Sorichetti, C.L. Matteo, O.A. Lambri, G.C. Manguzzi, L.M. Salvatierra, O. Herrero, IEEE Trans. Dielectr. Electr. Insul. 14 (2007) 1170.
[5] O.A. Lambri, L.M. Salvatierra, F.A. Sánchez, C.L. Matteo, P.A. Sorichetti, C.A. Celauro, Nucl. Instr. and Meth. B 237 (2005) 550.
[6] L.M. Salvatierra, O.A. Lambri, C.L. Matteo, P.A. Sorichetti, C.A. Celauro, R.E. Bolmaro, Nucl. Instr. and Meth. B 225 (2004) 297.
[7] R.R. Mocellini, O.A. Lambri, C.L. Matteo, J.A. García, G.I. Zelada-Lambri, P.A. Sorichetti, F. Plazaola, A. Rodríguez-Garraza, F.A. Sánchez, Polymer 50 (2009) 4696.
[8] Y.C. Jean, D.M. Schrader, P.E. Mallon (Eds.), Principles and Applications of Positron and Positronium Chemistry, World Science Publications, Singapore, 2003.
[9] M. Eldrup, D. Lightbody, J.N. Sherwood, Chem. Phys. 63 (1981) 51.
[10] H. Nakanishi, S.J. Wang, Y.C. Jean, in: S.C. Sharma (Ed.), Positron Annihilation Studies of Fluids, World Scientific, Singapore, 1988, p. 292.
[11] Y.Y. Wang, H. Nakanishi, Y.C. Jean, T.C. Sandreczki, J. Polym. Sci. B 28 (1990) 1431.
[12] J. Liu, Q. Den, Y.C. Jean, Macromolecules 26 (1993) 7149.
[13] Y.C. Jean, Nucl. Instr. Meth. B 56–57 (1991) 615.
[14] H.L. Li, Y. Ujihira, A. Nanasawa, Y.C. Jean, Polymer 40 (1999) 349.
[15] M. Welander, F.H.J. Maurer, Mat. Sci. Forum 105 (1992) 1811.
[16] X.S. Li, M.C. Boyce, J. Polymer. Sci. B 31 (1993) 869.
[17] C.L. Wang, F.H.J. Maurer, M. Eldrup, N.J. Pedersen, J. Chem. Phys. 108 (1998) 4654.
[18] T. Suzuki, Y. Oki, T. Numajiri, T. Miura, K. Kondo, N. Oshima, Y. Ito, Polymer (London-CHERIC) 37 (1996) 5521.
[19] T. Mura, Micromechanics of Defects in Solids, Martinus Nijhoff Publishers, New York, 1987.
[20] G.I. Zelada-Lambri, O.A. Lambri, P.B. Bozzano, J.A. García, C.A. Celauro, J. Nucl. Mater. 380 (2008) 111.
[21] J. Kansy, Nucl. Instr. Meth. A 374 (1996) 235.
[22] O.A. Lambri, A review on the problem of measuring non-linear damping and the obtainment of intrinsic damping, in: D. Walgraef, J. Martínez-Mardones, C.H. Wörner (Eds.), Materials Instabilities, World Scientific Publishing Co. Pte. Ltd., New Jersey, 2000, p. 249.
[23] L.D. Landau, E.M. Lifshitz, Theory of Elasticity, Reverté, Barcelona, 1969.
[24] A. Charlesby, Atomic Radiation and Polymers, Pergamon Press, Oxford, 1960.
[25] A. Charlesby, L. Callaghan, Phys. Chem. Solids 4 (1958) 306.
[26] N. Celette, I. Stevenson, J. Davenas, L. David, G. Vigier, Nucl. Instr. and Meth. B 185 (2001) 305.
[27] M. Celina, K.T. Gillen, J. Wise, R.L. Clough, Radiat. Phys. Chem. 48 (1996) 613.
[28] F.H. Winslow, M.Y. Hellman, W. Matreyek, S.M. Stills, Polym. Eng. Sci. 6 (1966) 273.
[29] I.M. Ward, Mechanical Properties of Solid Polymers, John Wiley & Sons, New York, 1990.
[30] O.A. Lambri, C.L. Matteo, R.R. Mocellini, P.A. Sorichetti, G.I. Zelada-Lambri, Propiedades Viscoelásticas y Eléctricas de Sólidos y Líquidos, Una Introducción a la Electro-Reología con sus Aplicaciones Tecnológicas, Editora de la Universidad Nacional de Rosario, Rosario, 2008.
[31] B.D. Cullity, Elements of X-ray Diffraction, Addison-Wesley Publishing Co., Reading, 1967.
[32] J. Baruchel, J.L. Hodeau, M.S. Lehmann, J.R. Regnard, C. Schlenker (Eds.), Neutron and Synchrotron Radiation for Condensed Matter Studies, Vol. II, HERCULES, Springer-Verlag, Les Editions de Physique, Berlin, 1994.
[33] G. Lachenal, I. Stevenson, N. Celette, Analyst 126 (2001) 2201.
[34] G. Lachenal, I. Stevenson, J. Near Infrared Spectrosc. 10 (2002) 279.